Journal of Computational Physics **174,** 473–488 (2001)
doi:10.1006/jcph.2001.6914, available online at http://www.idealibrary.com on IDEAL®

NOTE

Simple Modifications of Monotonicity-Preserving Limiters[1]

William J. Rider* and Len G. Margolin†

*Methods for Advanced Scientific Simulation, Computer and Computational Sciences Division, Los Alamos National Laboratory, MS D413; and †Center for Nonlinear Studies, Theoretical Division, Los Alamos National Laboratory, MS B258, Los Alamos, New Mexico 87545
E-mail: wjr@lanl.gov; len@lanl.gov

Received November 15, 2000; revised August 6, 2001

We present simple modifications of standard monotonicity-preserving limiters that provide either sign preservation or alternative bounding values for the resulting numerical schemes (e.g., that the solution remain between zero and one rather than preserving monotonicity). These limiters can be easily implemented in Godunov-type methods by modifying the reconstruction step of the algorithm. These modifications allow methods to achieve greater formal accuracy, for example by improving the first-order accuracy in the L_∞ norm. The greatest advantage of our approach is its natural extension to more than one spatial dimension, and to systems of equations without operator splitting.

Key Words: limiters; sign preserving; bounds preserving.

1. INTRODUCTION

Modern high-resolution Godunov schemes have proven to be effective techniques for solving a variety of fluid dynamic problems. Key elements in these methods are the nonlinear limiter functions that preserve monotonicity in the solution while allowing high-order accuracy in smooth flows. We note that linear monotone schemes are intrinsically first-order accurate [11, 20]. The lesser constraint of preserving monotonicity is essential for many problems, but may lead to excess numerical diffusion that will generally reduce accuracy. In one dimension the concept of monotonicity preservation and Total Variation Diminishing (TVD) are closely related, but TVD concepts do not extend to more than one dimension or to

[1] This work performed under the auspices of the U.S. Department of Energy by Los Alamos National Laboratory under Contract W-7405-ENG-36.

0021-9991/01

systems [11]. Throughout this paper we consider modifications to monotonicity-preserving schemes, and use a Godunov type of formalism [22, 23].

In this paper, we describe several simple modifications of standard limiters that relax the constraint of preserving monotonicity while enforcing weaker constraints. Our modified limiter functions improve the overall accuracy of simulations, and in particular can be tailored to better preserve the values of local maxima and minima. Further, these modifications are easily introduced into existing high-resolution multidimensional Godunov implementations.[2]

Earlier work in computational geophysics has demonstrated the effectiveness of sign-preserving methods (positive definite methods). Smolarkiewicz and co-workers introduced the MPDATA scheme, which preserves sign through the direct application of upwinding in a multistep procedure (see [l8, 13] and references therein). Bott introduced an alternative method that can be used to preserve the positive definiteness of the solution [3] (further discussion of this paper is contained in [17, 4]). Lin *et al*. describe one-dimensional limiters for computing sign-preserving or bounds-preserving solutions in geophysical applications [12] using a one-dimensional Godunov framework. These methods are discussed in a recent book by Durran [9], which also contains a brief discussion of how to implement both sign-preserving and bounds-preserving flux limiters. Our work differs in two important respects: the limiters naturally extend to a multidimensional form, and through a Goduov-type approach the method extends to hyperbolic systems of equations.

High-resolution Godunov schemes are based on three separate steps. First there is the reconstruction of a continuous solution of the dependent variable within a computational cell, based on the discrete values of the variable in the cell and its immediate neighborhood. This reconstruction necessarily leads to discontinuities at the cell interfaces. In the second step, these discontinuities are resolved via a Riemann solution between each of the adjacent cells to produce a single-valued solution at the interface and the associated flux. For a "first-order," classical Godunov method, this solution procedure is equivalent to simple upwinding (i.e., donor cell). However in high-resolution methods an intermediate step is required to construct the new cell values by temporally averaging the solution used in the Riemann problem. These fluxes produce new cell values that are the updated discrete solution, completing one time step.

Here we are only concerned with the first step, the reconstruction of the continuous solution. In the standard framework, we consider piecewise linear interpolation, where the local gradient within a cell is constructed from data in the immediate neighborhood of the cell and then modified by further multiplication with a scalar limiter function. The standard limiters that perserve monotonicity (equivalent to TVD in one dimension, but TVD does not extend to multiple dimensions) are nicely presented in [19, 11]. In this paper, we present new forms for the limiter function that are less restrictive. We demonstrate the performance of these limiters on idealized test problems in one and two dimensions and compare the results with those of the standard limiter.

An outline of this paper is as follows. In the next section, we briefly review the theory of the monotonicity preserving limiter. In Section 3 we describe a simple predictor–corrector

[2] The methods are nominally second order or higher, via linear or higher interpolation, but the term *high resolution* is used instead of *high order* because only first-order formal accuracy is achieved for discontinuous solutions. This means methods that have high accuracy in smooth flow are nonoscillatory and resolve discontinuities better than low-order methods.

algorithm to simulate linear advection. The algorithm uses linear interpolation in the predictor step, providing the framework to compare the standard monotonicity-preserving limiter with our new formulations. In Section 4, we present our modified limiter functions and apply them to a variety of one-dimensional test problems. We compare their performance to that of the monotonicity-preserving limiter on two idealized test problems: a Gaussian pulse exemplifying a smooth function and a square wave that represents a discontinuous function. We also show the impact of the new limiters on a higher order reconstruction by modifying a parabolic reconstruction. Last, we show two examples of using the sign-preserving limiter to simulate flows governed by the Euler equations of gas dynamics. In Section 5 we demonstrate the use of the new limiter functions in two spatial dimensions. We summarize our results in Section 6.

2. MONOTONICITY-PRESERVING LIMITERS

In the first phase of a high-resolution Godunov method, we reconstruct the continuous field within a cell $\Omega_{i,j}$ from the discrete set of cell-averaged values. For example, we might reconstruct the continuous field, ρ, within the cell from the discrete field $\bar{\rho}_{i,j} = \int_{\Omega_{i,j}} \rho(\mathbf{x})\, d\Omega$. Here the indices i, j indicate the cell center in a two-dimensional mesh and $\mathbf{x}$ is the coordinate vector.

For the reconstruction, we employ an interpolating function that is piecewise linear,

$$\rho(\mathbf{x}) = \bar{\rho}_{i,j} + \nabla\rho_{i,j} \cdot (\mathbf{x} - \bar{\mathbf{x}}_{i,j}), \quad \mathbf{x} \in \Omega_{i,j}. \tag{1}$$

To enforce the monotonicity of the continuous field, we augment the interpolation with a scalar limiter function, ϕ, that multiplies the gradient, $\nabla\rho_{i,j}$. This general approach to constructing a method and its limiter follows from Barth [1, 2] and has been applied to a variety of applications [7, 14]. In this paper, we only consider logically rectangular grids, although the methods should extend to more general grids. This approach also can be applied to the systematic construction of higher order expansions (an example is provided in Section 4).

The reconstructed field, now denoted $\hat{\rho}$ to emphasize its dependence on the limiter function, is given by

$$\hat{\rho}(\mathbf{x}) = \bar{\rho}_{i,j} + \phi_{i,j}\nabla\rho_{i,j} \cdot (\mathbf{x} - \bar{\mathbf{x}}_{i,j}), \quad \mathbf{x} \in \Omega_{i,j}. \tag{2}$$

The scalar limiter function can be defined as

$$\phi_{i,j} = \min\left(1,\ \frac{\Delta\bar{\rho}^{\max}_{i,j}}{\Delta_{\max}\rho_{i,j}},\ \frac{\Delta\bar{\rho}^{\min}_{i,j}}{\Delta_{\min}\rho_{i,j}}\right) \tag{3}$$

(see [8]). Here $\Delta\bar{\rho}^{\max}_{i,j} = \bar{\rho}^{\max}_{i,j} - \bar{\rho}_{i,j}$, where $\bar{\rho}^{\max}_{i,j}$ is the maximum of the local data usually taken in a neighborhood of all the cells adjacent to $\Omega_{i,j}$. Also $\Delta_{\max}\rho_{i,j}$ is the maximum value of the reconstructed values within the cell *without limiting* minus the cell-average value (i.e., $\max(\rho_{i,j}) - \bar{\rho}_{i,j}$; this value will occur at a cell edge for a linear reconstruction). The terms $\Delta\bar{\rho}^{\min}_{i,j}$ and $\Delta_{\min}\rho_{i,j}$ are defined analogously. This definition of the limiter provides the reconstruction with the property of local boundedness.[3] The modifications to the limiter

[3] $\bar{\rho}^{n+1}_{i,j} \in [\bar{\rho}^{\min}_{i,j}, \bar{\rho}^{\max}_{i,j}]\mathbf{x} \in \Omega_{i,j}$.

that we describe in this paper can be implemented via simply redefining $\bar{\rho}_{i,j}^{\max}$ and $\bar{\rho}_{i,j}^{\min}$. In particular we relax the constraints on these quantities; in this sense our new limiters are less restrictive and allow higher order accuracy to be achieved.

In one dimension, we can explicitly display the limiter function (3) in terms of an unspecified gradient. The limited piecewise linear interpolant is

$$\hat{\rho}_j(x) = \bar{\rho}_j + \phi_j \frac{\partial \rho}{\partial x_j}\ (x - \bar{x}_j).$$

Then the edge values in a cell are given by

$$\hat{\rho}_j\left(x_{j\pm\frac{1}{2}}\right) = \bar{\rho}_j + \phi_j \frac{\partial \rho}{\partial x_j}\left(x_{j\pm\frac{1}{2}} - \bar{x}_j\right).$$

The quantities required by the limiter function are easily computed:

$$\bar{\rho}_j^{\max} = \max(\bar{\rho}_{j-1}, \bar{\rho}_j, \bar{\rho}_{j+1}), \tag{4}$$

$$\bar{\rho}_j^{\min} = \min(\bar{\rho}_{j-1}, \bar{\rho}_j, \bar{\rho}_{j+1}), \tag{5}$$

$$\Delta_{\max}\rho_j = \max\left(\rho_j\left(x_{j-\frac{1}{2}}\right), \rho_j\left(x_{j+\frac{1}{2}}\right)\right) - \bar{\rho}_j,$$

and

$$\Delta_{\min}\rho_j = \bar{\rho}_j - \min\left(\rho_j\left(x_{j-\frac{1}{2}}\right), \rho_j\left(x_{j+\frac{1}{2}}\right)\right).$$

Now consider the case where the mesh has constant spacing Δx and where the solution increases to the right. Then $\bar{\rho}_j^{\max} = \bar{\rho}_{j+1}$ and $\bar{\rho}_j^{\min} = \bar{\rho}_{j-1}$, $\Delta_{\max}\rho_j = \frac{1}{2}\Delta x \partial\rho/\partial x_j$, and $\Delta_{\min}\rho_j = \frac{1}{2}\Delta x \partial\rho/\partial x_j$. Thus we can explicitly write the limiter function in terms of the (as yet unspecified) gradient

$$\phi_j = \min\left(1, \frac{2(\bar{\rho}_{j+1} - \bar{\rho}_j)}{\Delta x \partial\rho/\partial x_j}, \frac{2(\bar{\rho}_j - \bar{\rho}_{j-1})}{\Delta x \partial\rho/\partial x_j}\right). \tag{6}$$

3. LIMITED FROMM SCHEME

To illustrate the use of the standard limiter and the new modifications that we describe, we consider the simple example of advection of a scalar field ρ by a constant velocity $a = 1$ in one space dimension,

$$\frac{\partial \rho}{\partial t} + a\frac{\partial \rho}{\partial x} = 0. \tag{7}$$

We employ a numerical algorithm based on forward-time integration. For the basic scheme with limiting, we first define upwind values evaluated at half-time levels using

$$\hat{\rho}_{j+\frac{1}{2}}^{n+\frac{1}{2}} = \hat{\rho}_{j+\frac{1}{2}}^{n} - \frac{\Delta t}{2} a \phi_j \frac{\partial \rho}{\partial x_j}, \tag{8}$$

or, equivalently,

$$\hat{\rho}_{j+\frac{1}{2}}^{n+\frac{1}{2}} = \hat{\rho}_{j+\frac{1}{2}}^{n} - \frac{\Delta t}{2\Delta x} a\left(\hat{\rho}_{j+\frac{1}{2},-}^{n} - \hat{\rho}_{j-\frac{1}{2},+}^{n}\right),$$

TABLE I
The Accuracy of Unlimited Fromm Scheme on a Gaussian Pulse Advected with the Scalar Wave Equation

Norm	Error 20	Rate 20–40	Error 40	Rate 40–80	Error 80
L_1	2.3×10^{-2}	2.39	4.4×10^{-3}	2.29	9.1×10^{-4}
L_2	3.0×10^{-2}	2.32	6.0×10^{-3}	2.29	1.2×10^{-3}
L_∞	6.5×10^{-2}	2.29	1.3×10^{-2}	2.32	2.7×10^{-3}

Note. A CFL number of 0.3 is used with periodic boundary conditions for a single transit of the grid. Results shown at $t = 1.0$.

where the cell-edge values $\rho^n_{j+\frac{1}{2}}$ are reconstructed from the cell-centered data via (2) and evaluated using the cell j reconstructions. The new time values are then calculated as

$$\bar{\rho}^{n+1}_j = \bar{\rho}^n_j - \frac{a\Delta t}{\Delta x}\left(\hat{\rho}^{n+\frac{1}{2}}_{j+\frac{1}{2}} - \hat{\rho}^{n+\frac{1}{2}}_{j-\frac{1}{2}}\right). \tag{9}$$

To actualize the algorithm, we must specify the form of the gradient, which is used directly in (8) and also indirectly in reconstructing the cell-edge values. The gradient is also used in the limiter function, if employed. For example, if we were to use piecewise linear interpolation for the cell-edge value $\hat{\rho}^n_{j+\frac{1}{2}}$, and if the gradients were calculated at the cell edges, then a predictor–corrector Lax–Wendroff method would result. However throughout this paper we use a cell-centered gradient (Fromm's scheme) [21]; for constant mesh spacing, this gradient has the form

$$\frac{\partial \rho}{\partial x_j} \approx \frac{\bar{\rho}^n_{j+1} - \bar{\rho}^n_{j-1}}{2\Delta x} + \mathcal{O}(\Delta x^3). \tag{10}$$

We use two standardized problems—advection of a Gaussian pulse and of a square wave—to do basic testing of our methods. Our smooth problem is the transport of the Gaussian pulse $\rho = \exp[-30(x - \frac{1}{2})^2]$ on the interval $x \in [0, 1]$ which allows us to evaluate the ability of a scheme (and in particular a limiter function) to preserve the amplitudes of local maxima. The square wave allows us to evaluate the effects of relaxing monotonicity-preserving constraints at discontinuities. We also run the Gaussian pulse at several resolutions to estimate the rate of convergence. We run all the one-dimensional problems with a CFL number of 0.3, and with periodic boundary conditions using 20 cells. The Gaussian

TABLE II
The Accuracy of Basic Monotonicity-Preserving Limiter on a Gaussian Pulse Advected with the Scalar Wave Equation

Norm	Error 20	Rate 20–40	Error 40	Rate 40–80	Error 80
L_1	3.1×10^{-2}	2.02	6.9×10^{-3}	2.18	1.7×10^{-3}
L_2	4.7×10^{-2}	1.89	1.2×10^{-2}	1.95	3.3×10^{-3}
L_∞	1.2×10^{-1}	1.53	4.4×10^{-2}	1.42	1.5×10^{-2}

Note. A CFL number of 0.3 is used with periodic boundary conditions for a single transit of the grid. Results shown at $t = 1.0$.

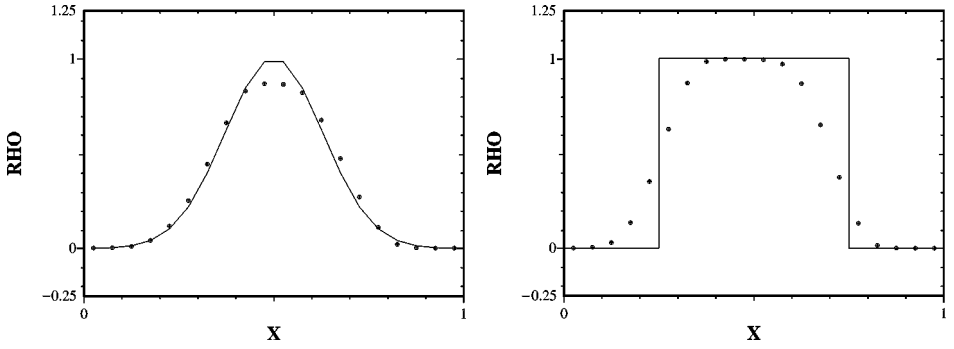

FIG. 1. The performance of the basic monotone limiter on several simple tests. Both use 20 cells and a CFL number of 0.3 with periodic boundary conditions for a single transit of the grid. Results shown at $t = 1.0$. (Left) A Gaussian $\exp(-30(x - \frac{1}{2})^2)$. (Right) Square wave.

pulse problems are repeated with 40 and 80 cells. The final time step of the calculation is modified to be small enough so that the solution is output at a time exactly equal to 1.0. In Table I we show how this method performs without any limiter to provide a baseline for the best performance one can reasonably expect in terms of accuracy. These norms are defined as follows: the error per cell is $E_j = V_j(U_{exact,j} - U_j)$, where V_j is the volume of the cell (we use $V_j = \Delta x$ in one dimension), $L_1 = \sum_j |E_j|$, $L_2 = \sqrt{\sum_j E_j^2}$, and $L_\infty = \max_j E_j$.

As a basis for later comparison with our modified limiters, we show the performance of the basic limiter (6) applied with our scheme (8), (9), and (10) on our two chosen problems. The accuracy of the method for advecting a Gaussian pulse for three different norms is recorded in Table II. The method is second-order accurate in L_1, is weakly second order in L_2, but is less than second order in L_∞. We show that the degradation of the peak amplitude can be reduced with our modified limiters. The solution for the square wave is monotone and the wave remains fairly symmetric. A graphical depiction of performance is shown in Fig. 1, where the computed solution using the basic limiter is compared to the analytic solution.

4. MODIFIED LIMITER FUNCTIONS

4.1. Sign-Preserving Limiter

Our first modification represents a relaxation of the standard limiter that produces a sign-preserving scheme. We dispense with the use of $\overline{\rho}_{i,j}^{\max}$ in the limiter and set $\overline{\rho}_{i,j}^{\min}$ to a global value of zero. The limiter is now

$$\phi = \min\left(1, \frac{\Delta\overline{\rho}^{\min}}{\Delta_{\min}\rho}\right), \tag{11}$$

which will produce results that do not fall below zero.

Let us examine the performance of this modification on our two standard problems. As shown in Table III, the accuracy of the scheme is improved significantly over the standard monotonicity-preserving result. The solution is now strongly second-order accurate in all three norms examined. Figure 2 shows that a new maxima is produced in the square wave, but the width of the steep transitions associated with the square wave remains almost

TABLE III
The Accuracy of Our Sign-Preserving Limiter on a Gaussian Pulse Advected with the Scalar Wave Equation

Norm	Error 20	Rate 20–40	Error 40	Rate 40–80	Error 80
L_1	2.2×10^{-2}	2.29	4.4×10^{-3}	2.32	9.1×10^{-4}
L_2	3.0×10^{-2}	2.36	6.0×10^{-3}	2.31	1.2×10^{-3}
L_∞	6.6×10^{-2}	2.33	1.3×10^{-2}	2.30	2.7×10^{-3}

identical to earlier results. Furthermore the symmetry of the square wave has improved, reproducing the general phase error properties of Fromm's scheme.

4.2. Global Minimum/Maximum Limiter

Consider a small variation of the problem of advecting the square wave, in which one adds a constant background to the field. Application of the sign-preserving limiter to this problem would show undershoots developing at the leading and trailing edges of the wave. Of course these undershoots were precluded in the absence of the background.

This leads us to consider a generalization of the sign-preserving limiter, in which one enforces an arbitrary arbitrarily chosen value of the global minimum, not necessarily zero. We note a similar strategy has been developed to apply a sign-preserving advection scheme to the momentum equation by [18]. This technique can be equally well applied to enforce an arbitrary global maximum as well. Finally, the global minimum and global maximum can be enforced simultaneously. An example of a situation in which this limiter would be useful is the advection of a species fraction, which is bounded physically between zero and one.

To implement this global minimum/maximum limiter, we set the values of $\bar{\rho}_{i,j}^{\max}$ and $\bar{\rho}_{i,j}^{\min}$ globally. We have applied this limiter to our test problems, choosing the global values of of $\bar{\rho}_{i,j}^{\max} = 1$ and $\bar{\rho}_{i,j}^{\min} = 0$.

Table IV shows that the accuracy of the solution is nearly identical to the sign-preserving limiter. That is, the solution is second-order accurate in all norms. The results reproduce the monotone results associated with the basic limiter shown in Fig. 3; in particular the spurious new maximum of the square wave generated by the sign-preserving limiter is gone. This

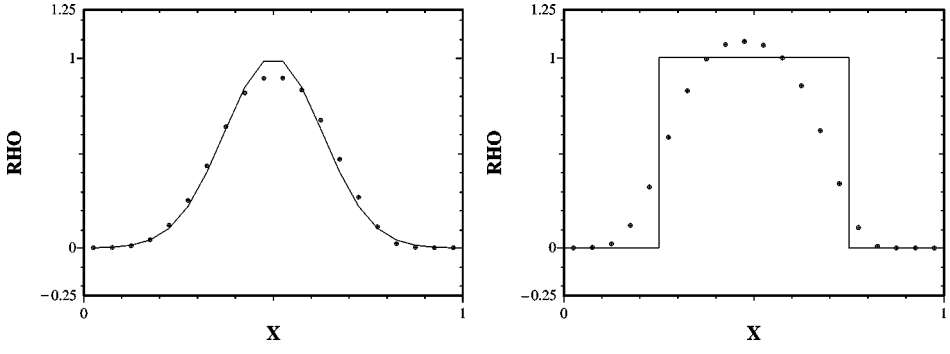

FIG. 2. The results using the sign-preserving limiter for a Gaussian pulse (left) and a square wave (right).

TABLE IV
The Accuracy of Our Bounds-Preserving Limiter on a Gaussian Pulse Advected with the Scalar Wave Equation

Norm	Error 20	Rate 20–40	Error 40	Rate 40–80	Error 80
L_1	2.2×10^{-2}	2.29	4.5×10^{-3}	2.32	9.1×10^{-4}
L_2	3.0×10^{-2}	2.36	6.0×10^{-3}	2.31	1.2×10^{-3}
L_∞	6.6×10^{-2}	2.32	1.3×10^{-2}	2.31	2.6×10^{-3}

scheme gives high accuracy for smooth flow without compromising the physical nature of the solution.

4.3. Higher-Order Reconstructions

To demonstrate the performance of our modifications in algorithms different from those discussed previously, we turn to discontinuous Galerkin methods [5, 6]. Below we show the impact of the sign-preserving limiter on results found with a parabolic basis (DG(2) for a second-order Legendre polynomial) integrated with a third-order TVD Runge–Kutta method [16]. Overall we expect third-order accuracy from the method. As we see, the accuracy is far greater than from the limited Fromm scheme given before. In this case, the limiter is computed as before and applied to all terms in the reconstruction except the constant (the cell-average value).

First, we show results for the scheme using the standard limiter on our two chosen problems. Everything is the same as earlier, except the CFL number is now 0.1 to conservatively satisfy the more restrictive stability condition of this method (CFL $= 0.2$). Table V shows that the method with the standard limiter has errors of the same magnitude as the Fromm scheme with our modified limiter. This is indicative of the high accuracy from the unlimited scheme. In Fig. 4 we show the polynomial reconstructions defined by the evolving basis with the dashed line. These are most effectively displayed in this form.

Now we show the results of RK3–DG(2) with the sign-preserving limiter. Table VI documents both the high intrinsic accuracy of this method and the great improvement in accuracy achievable using the sign-preserving limiter. This improvement is also evident in the plots of the solution for these two problems shown in Fig. 5.

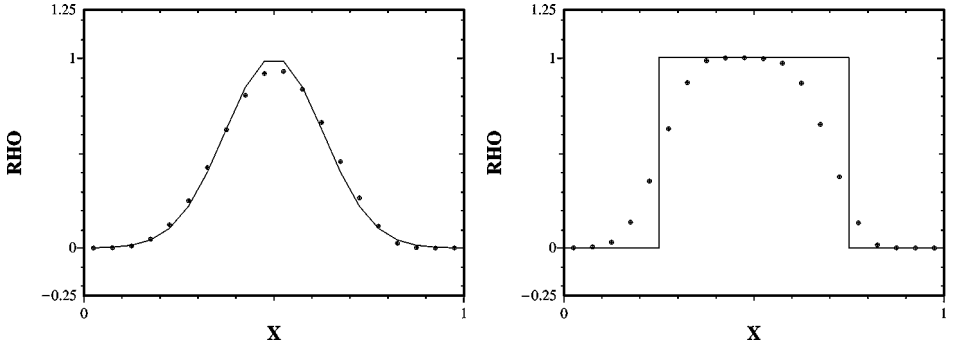

FIG. 3. The results using the bounded limiter on a Gaussian pulse (left) and a Square wave (right).

TABLE V
The Accuracy of the Standard Limiter on a Gaussian Pulse Advected with the Scalar Wave Equation Using the RK3–DG(2) Method

Norm	Error 20	Rate 20–40	Error 40	Rate 40–80	Error 80
L_1	7.9×10^{-3}	2.66	1.3×10^{-3}	2.68	1.2×10^{-4}
L_2	1.5×10^{-2}	2.16	3.4×10^{-3}	2.16	7.6×10^{-4}
L_∞	4.2×10^{-2}	1.73	1.3×10^{-2}	1.79	3.6×10^{-3}

Note. The dashed line displays the piecewise parabolic polynomial reconstruction evolved with the flow.

TABLE VI
The Accuracy of the Sign-Preserving Limiter on a Gaussian Pulse Advected with the Scalar Wave Equation Using the RK3–DG(2) Method

Norm	Error 20	Rate 20–40	Error 40	Rate 40–80	Error 80
L_1	2.0×10^{-4}	3.27	2.1×10^{-5}	3.27	3.0×10^{-6}
L_2	2.7×10^{-4}	3.31	2.7×10^{-5}	3.31	4.3×10^{-6}
L_∞	6.4×10^{-4}	3.29	6.5×10^{-5}	2.00	1.6×10^{-6}

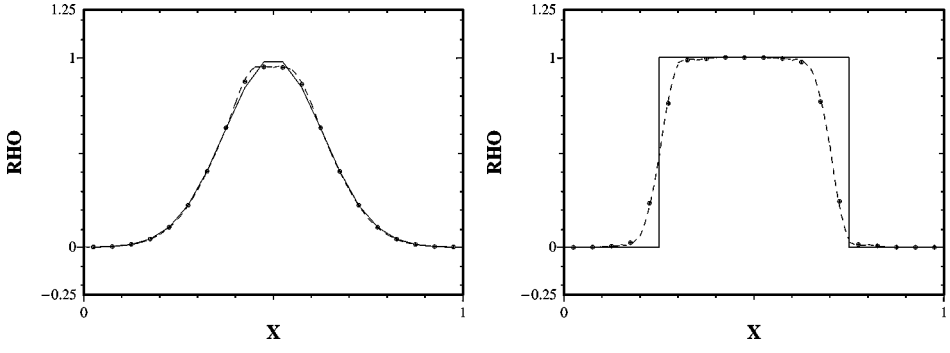

FIG. 4. The RK3–DG(2) results using the standard limiter on a Gaussian pulse (left) and Square wave (right).

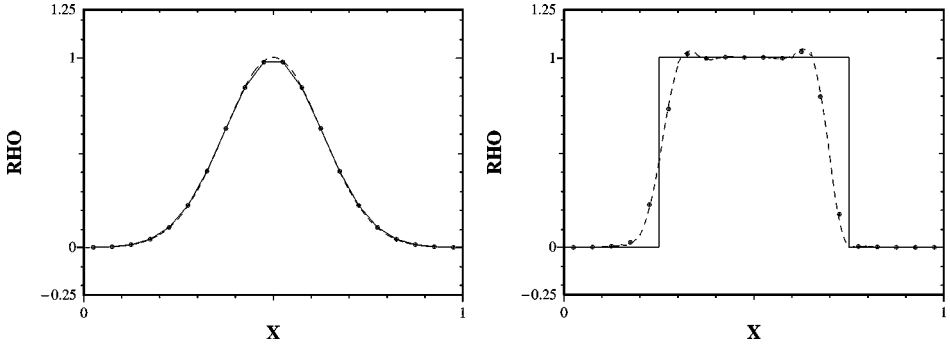

FIG. 5. The RK3–DG(2) results using the sign-preserving limiter on a Gaussian pulse (left) and a square wave (right).

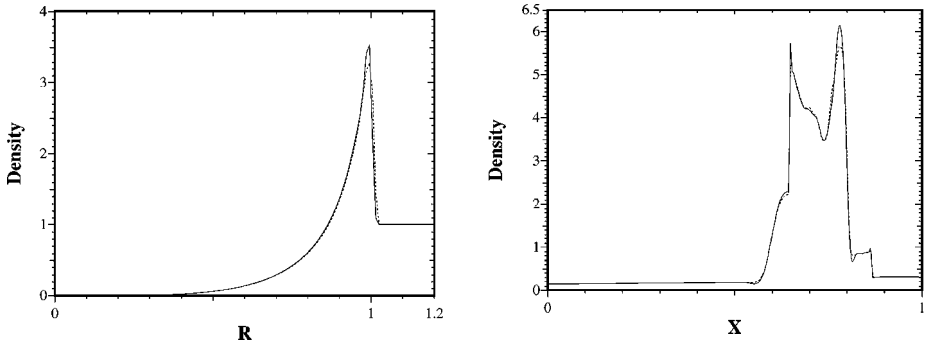

FIG. 6. Results obtained using the sign-preserving limiter on the Euler equations of gas dynamics for two blast wave problems. In the Sedov problem 120 cells are used and 400 cells are used in the blast wave problem. Both problems are run at a maximum CFL number of 0.8. (Left) The Taylor–Sedov blast wave. (Right) Interacting blast waves.

4.4. Euler Equations of Gas Dynamics

As a final example in one dimension, we apply one of our modified limiters to a system of equations. This example is intended to illustrate the robustness of the modification and its extensibility to systems of equations. We test the method on simulating the Euler equations of gas dynamics by modifying the limiters used in the scheme described by Rider [15] to be sign-preserving rather than monotonicity preserving. All other features of the method described in [15] are unchanged.[4]

The solution is shown in Fig. 6 for the Taylor–Sedov blast wave [10] and the interacting blast wave problem [24]. In both cases, the modified limiter retains peak values better while allowing small oscillations in the interacting blast wave problems. In this figure, the dashed line displays the solution computed with the standard monotonicity-preserving limiter. In the Sedov problem, the modified limiter changes the peak value in density from 3.26 to 3.52 (the correct value is 4). For the interacting blast waves the right peak increases in value from 5.64 to 6.12, and the left peak overshoots its converged value, but converges under mesh refinement (the converged value is $\approx$6.5). More important, the scheme is a simple modification of the base method and is quite robust despite the complex nature and severity of the shocks in these problems.

5. IMPLEMENTATION IN TWO DIMENSIONS

We can easily extend each of the modifications of the previous section to multiple dimensions. In general terms, we expand the neighborhood for the calculation of $\bar{\rho}_{i,j}^{\max}$ and $\bar{\rho}_{i,j}^{\min}$ to include all the data within the support of $\nabla\rho$. For our tests in two dimensions, we use a Hancock scheme for the multidimensional time integration [20], and a nine-cell basis for $\nabla\rho$. For example, the x-component of the gradient is written

$$\frac{\partial\rho}{\partial x} \approx \frac{\bar{\rho}_{i+1,j-1} + 4\bar{\rho}_{i+1,j} + \bar{\rho}_{i+1,j+1} - \bar{\rho}_{i-1,j-1} - 4\bar{\rho}_{i-1,j} - \bar{\rho}_{i-1,j+1}}{12\Delta x} + \mathcal{O}(\Delta x^3, \Delta x \Delta y^2). \tag{12}$$

[4] The scheme described there uses Hancock's method, a monotonicity-preserving van Leer differencing coupled with an adaptive two-shock Riemann solver.

Thus the reconstruction and the limiter function will depend on the data $\bar{\rho}_{i\pm1,j\pm1}$ and the construction of our modified limiters will involve only analogous changes to the definitions of the maximum and minimum values.

In this section, we apply each of our modified limiters to three separate tests. First there is a Gaussian "hill" rotated around the unit square, which we use to test the ability of the various limiters to preserve the amplitude of peaks. Second, there is a sine wave advected at an angle across a periodic domain, which we run at three resolutions to test convergence rate. Third, there is a "slotted cylinder" rotated around the unit square, which we use to test the effects of the limiters on steep (initially discontinuous) pulses.

Our first two-dimensional test is the Gaussian hill $\rho = \exp[\sqrt{(x-0.5)^2+(y-0.75)^2}/0.15]$, rotated once around the unit domain using a CFL number of 0.5. The CFL number is computed at the minimum value of $\Delta x/(|v_x|+|v_y|)$. The rotational velocity field is defined by $v_x = -2(y-\frac{1}{2})$ and $v_y = 2(x-\frac{1}{2})$. The domain is covered with 100×100 cells. After one revolution, the base method with the standard monotonicity-preserving limiter (3) produces a peak value of 0.824, a loss of nearly 14% from the initial value of 0.950. As before, the sign-preserving and bounded limiters give the same results, both reducing the loss of amplitude to less than 10%, producing a peak value of 0.858. These results are plotted in Fig. 7.

To quantify solution order and convergence rate, we advect a two-dimensional sine wave $\rho(x,y) = \sin(\pi x)\sin(\pi y)$ on a square periodic grid of unit length; the advective velocity makes an angle of 45° to the mesh lines. We measure the error after one full period. For a CFL number of 0.5, Fromm's scheme has (theoretically) a third-order rate of convergence. In Table VII the order of accuracy is shown for three of the limiter functions. For the monotonicity-preserving limiter, the convergence rate is essentially third order in L_1, but significantly decreases in L_2 and falls below second order in L_∞. The sign- or bounds-preserving limiters give third-order accuracy in both L_1 and L_2, and higher than second-order accuracy in L_∞. Note also that the overall error of the sign- or bounds-preserving schemes in L_1 is only slightly better than that of the monotonicity-preserving scheme; however in L_2 the advantage is about a factor of five, while in L_∞, the advantage is nearly a factor of 40.

We repeat these calculations at a small Courant number, 0.05. A small Courant number is difficult for two reasons: the larger number of time steps that allow discrete errors to accumulate and that upwind methods perform quite well at large Courant numbers (often being exact at a Courant number of one; i.e., they are characteristic). These results are summarized in Table VIII. The new limiters still have an advantage, but their effectiveness is reduced somewhat. The L_1, L_2, and L_∞ errors are reduced over the base scheme.

Lastly, we show two-dimensional results for a discontinuous solution. We rotate the slotted cylinder [25] once around the unit domain using a CFL number of 0.5. The initial peak value is 1.000. As shown in Fig. 8, the peak value of the monotonicity-preserving scheme is somewhat eroded at 0.968; for the sign-preserving limiter the peak is 1.136, and the bounded limiter yields the best result, maintaining a peak value of 0.9996 without producing unphysical overshoots. The sign-preserving limiter produces fairly large overshoots, but does reduce the erosion of the "bridge" between the two sides of the cylinder.

When the CFL number is reduced to 0.05 the relative advantage of the new limiters is reduced, but still clear. The base scheme gives a peak value of 0.946 while the sign-preserving limiter allows overshoots to 1.118. The bounded limiter retains the maximum value at 0.999. The two new limiters reduce the L_1 error by 5 and 2.5%, respectively. They also decrease to overall size of other errors by relatively small amounts.

TABLE VII
The Accuracy of the Limiters for a Periodic Sine Wave Translated at 45 Degrees for One Period in Two Dimensions with a CFL Number of 1/2

Norm	Error 50 × 50	Rate	100 × 100	Rate	200 × 200
$L_{1,\text{mono}}$	1.3×10^{-3}	2.88	1.8×10^{-4}	2.98	2.3×10^{-5}
$L_{2,\text{mono}}$	2.2×10^{-3}	2.37	4.3×10^{-4}	2.38	8.2×10^{-5}
$L_{\infty,\text{mono}}$	1.8×10^{-2}	1.65	5.8×10^{-3}	1.54	2.0×10^{-3}
$L_{1,\text{sign}}$	9.8×10^{-4}	2.99	1.2×10^{-4}	3.00	1.5×10^{-5}
$L_{2,\text{sign}}$	1.1×10^{-3}	2.99	1.4×10^{-4}	3.00	1.7×10^{-5}
$L_{\infty,\text{sign}}$	1.6×10^{-3}	2.61	2.7×10^{-4}	2.30	5.4×10^{-5}
$L_{1,\text{bound}}$	9.8×10^{-4}	2.99	1.2×10^{-4}	3.00	1.5×10^{-5}
$L_{2,\text{bound}}$	1.1×10^{-3}	2.99	1.4×10^{-4}	3.00	1.7×10^{-5}
$L_{\infty,\text{bound}}$	1.6×10^{-3}	2.61	2.7×10^{-4}	2.30	5.4×10^{-5}

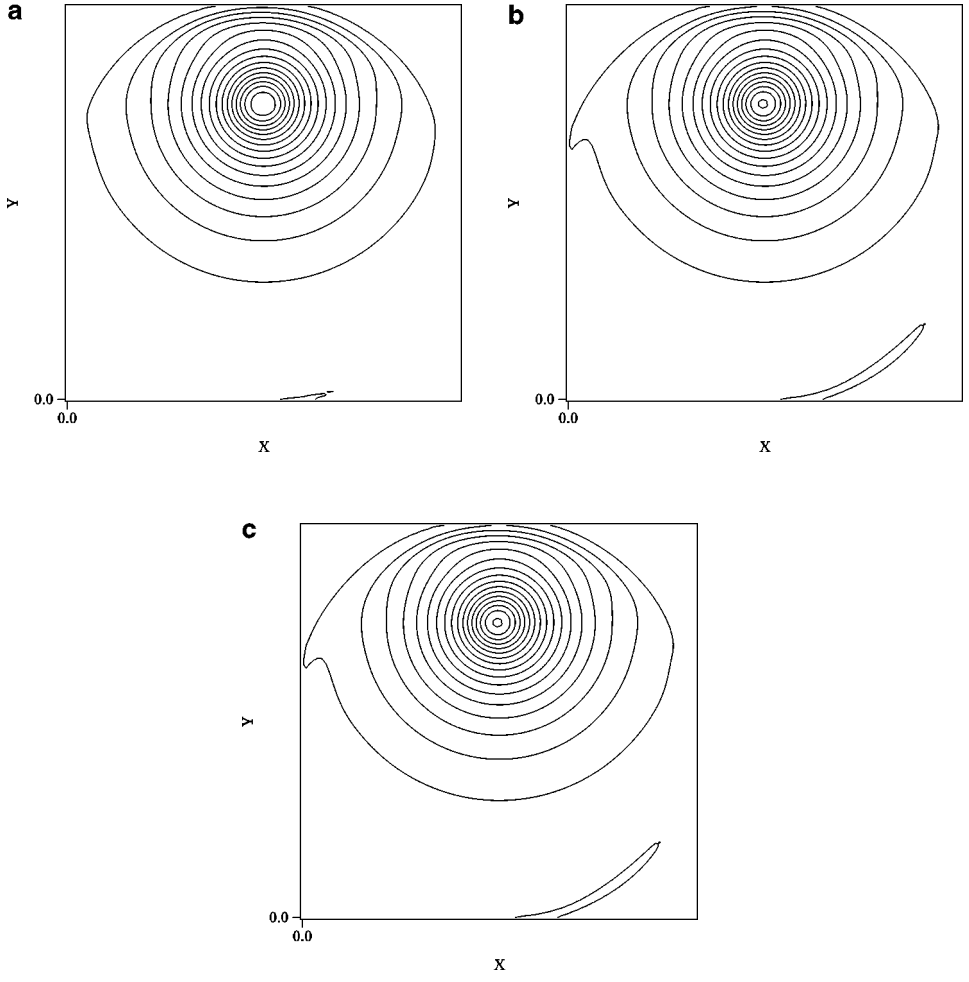

FIG. 7. A two-dimensional example of the four limiters showing the rotation of a Gaussian pulse through one complete revolution (a) Basic limiter; (b) sign-preserving limiter; and (c) bounds-preserving limiter.

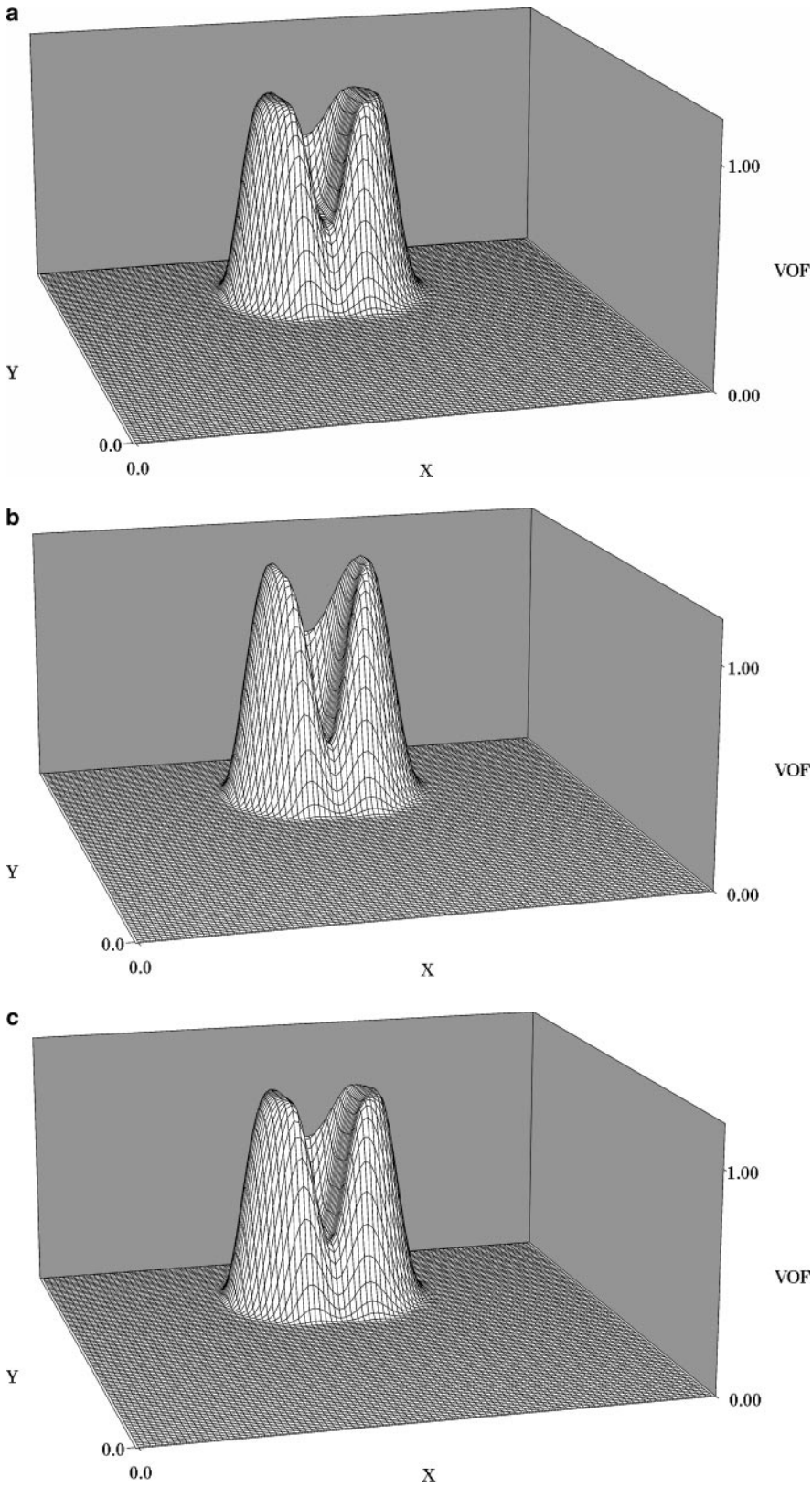

FIG. 8. A two-dimensional example of the three limiters showing the rotation of the slotted cylinder. (a) Basic limiter; (b) sign-preserving limiter; and (c) bounds-preserving limiter.

TABLE VIII
The Accuracy of the Limiters for a Periodic Sine Wave Translated at 45 Degrees for One Period in Two Dimensions with a CFL Number of 1/20

Norm	Error 50×50	Rate	100×100	Rate	200×200
$L_{1,\text{mono}}$	2.6×10^{-3}	2.16	5.8×10^{-4}	2.16	1.3×10^{-4}
$L_{2,\text{mono}}$	4.0×10^{-3}	2.23	8.5×10^{-4}	2.16	1.9×10^{-4}
$L_{\infty,\text{mono}}$	2.7×10^{-2}	1.65	8.6×10^{-3}	1.56	2.9×10^{-3}
$L_{1,\text{sign}}$	2.2×10^{-3}	2.13	4.9×10^{-4}	2.06	1.2×10^{-4}
$L_{2,\text{sign}}$	2.5×10^{-3}	2.18	5.6×10^{-4}	2.06	1.3×10^{-4}
$L_{\infty,\text{sign}}$	4.7×10^{-3}	2.31	9.5×10^{-4}	2.17	2.1×10^{-4}
$L_{1,\text{bound}}$	2.2×10^{-3}	2.13	4.9×10^{-4}	2.06	1.2×10^{-4}
$L_{2,\text{bound}}$	2.5×10^{-3}	2.18	5.6×10^{-4}	2.06	1.3×10^{-4}
$L_{\infty,\text{bound}}$	4.7×10^{-3}	2.31	9.5×10^{-4}	2.17	2.1×10^{-4}

6. SUMMARY

In this paper we have constructed new flux limiter functions for use in conjunction with high-resolution Godunov solvers. These limiters relax the relatively stringent condition of preserving monotonicity, while enforcing less-restrictive conditions. Furthermore these new limiters are readily implemented in the standard framework of monotonicity-preserving schemes. Moreover, these schemes can be applied via a Godunov type of algorithm and are applicable to complex systems of equations. We have provided several examples from gas dynamics to show the robustness of this approach.

Although monotonicity-preserving algorithms are sometimes required to prevent unphysical oscillations in the solution, there are many simulations where the preservation of monotonicity is not essential. We have shown that the numerical diffusion associated with monotonicity-preserving algorithms can significantly degrade a solution, eroding the amplitude of local maxima and decreasing both the overall accuracy and rate of convergence of solutions. In such cases, we have also shown that less-restrictive conditions such as sign preservation, or more generally the preservation of global minimum or maximum values, produce an improved result in the sense of better accuracy.

However, use of these limiters will be potentially oscillatory near steep or discontinuous profiles, and so caution must be exercised to determine which features of the flow the user deems more important. As a final example we show the performance of the standard and bounds-preserving limiter on a slightly more complex wave form. The double step has an intermediate step that does not influence the choice for the global bounds. The solutions are seen in Fig. 9 and aside from small oscillations around the intermediate jump there is little difference. If such oscillations are not acceptable, the standard limiter should be used. In terms of error, the L_1 norms are quite close, but are lower for the new limiter over the lower half of the domain, $\boldsymbol{x} \in [0, 0.5]$, and lower for the standard limiter for $\boldsymbol{x} \in [0.5, 1]$. This might be expected given the nature of the problem and the chosen bounds.

The main results of this paper are presented in Section 3; there we showed how to modify the standard monotonicity-preserving limiter function in one spatial dimension through the simple process of redefining two of the parameters on which the limiter depends—the values of the local maximum and minimum values $\bar{\rho}^{\max}$ and $\bar{\rho}^{\min}$. The less we restrict these values, the less diffusive is the resulting scheme. Also in this section we explicitly demonstrated the

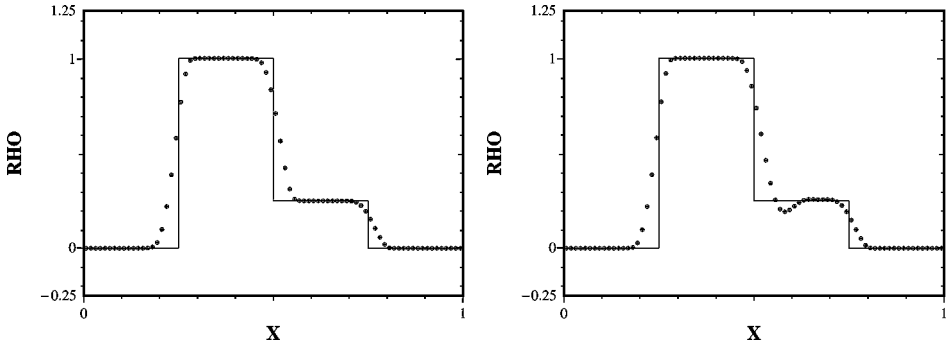

FIG. 9. The performance of the basic monotone and bounds-preserving limiter on a double step waveform. For the bounds-preserving limiter the global bounds are $\overline{\rho}^{\min} = 0$ and $\overline{\rho}^{\max} = 1$. Both use 80 cells and a CFL number of 0.3, with periodic boundary conditions for a single transit of the grid. Results shown at $t = 1.0$. (Left) Standard limiter and (Right) bounds-preserving limiter.

performance of each of our modified limiters. In Section 4 we described the generalization of our constructions to two spatial dimensions, and computationally verified their behavior.

In summary, we have found that the limiter based on choosing global values for $\overline{\rho}^{max}$ and $\overline{\rho}^{\min}$ is particularly effective in problems for which meaningful choices of these values can be made. One important example is the advection of species fractions, where on physical grounds, one can choose $\overline{\rho}^{\max} = 1$ and $\overline{\rho}^{\min} = 0$. More generally, the ability to enforce physical constraints other than monotonicity through simple modifications of an algorithm should be explored further.

REFERENCES

1. T. J. Barth, *Aspects of Unstructured Grids and Finite-Volume Solvers for Euler and Navier–Stokes Equations*, VKI/NASA/AGARD Special Course on Unstructured Grid Methods for Advection Dominated Flows, AGARD Publ. R-787 (Von Karmen Institute for Fluid Dynamics, Belguim, 1995).
2. T. J. Barth, *Parallel CFD Algorithms on Unstructured Meshes*, VKI/NASA/AGARD Lecture Series on Parallel Computing, AGARD Publ. R-807 (Von Karmen Institute for Fluid Dynamics, Belguim, 1995).
3. A. Bott, A positive definite advection scheme obtained by nonlinear renormalization of the advective fluxes, *Mon. Weather Rev.* **117**, 1006 (1989).
4. A. Bott, Reply to Smolarkiewicz's comment, *Mon. Weather Rev.* **117**, 2633 (1989).
5. B. Cockburn and C.-W. Shu, TVB Runge–Kutta local projection discontinuous Galerkin finite-element method for conservation-laws. 2. General framework, *Math. Comput.* **52**, 411 (1989).
6. B. Cockburn and C.-W. Shu, The Runge–Kutta discontinuous Galerkin method for conservation laws. V. Multidimensional systems, *J. Comput. Phys.* **141**, 199 (1998).
7. D. DeZeeuw and K. G. Powell, An adaptively refined cartesian mesh solver for the Euler equations, *J. Comput. Phys.* **104**, 56 (1993).
8. J. K. Dukowicz and J. W. Kodis, Accurate conservative remapping (rezoning) for arbitrary Lagrangian–Eulerian computations, *SIAM J. Sci. Stat. Comput.* **8**, 305 (1987).
9. D. R. Durran, *Numerical Methods for Wave Equations in Geophysical Fluid Dynamics* (Springer-Verlag, Berlin/New York, 1999).
10. B. Fryxell, K. Olson, P. Ricker, F. X. Timmes, M. Zingale, D. Q. Lamb, P. MacNeice, R. Rosner, J. W. Truran, and H. Tufo, Flash: An adaptive mesh hydrodynamics code for modeling astrophysical thermonuclear flashes, *Astrophys. J. Suppl. Ser.* **131**, 273 (2000).
11. R. J. Leveque, *Numerical Methods for Conservation Laws* (Birkhäuser Boston, Cambridge, MA, 1990).

12. S. J. Lin, W. C. Chao, Y. C. Sud, and G. K. Walker, A class of the van Leer-type transport schemes and its application to the moisture transport in a general circulation model. *Mon. Weather Rev.* **122**, 1575 (1994).
13. L. G. Margolin and P. K. Smolarkiewicz, Antidiffusive velocities for multipass donor cell advection, *SIAM J. Sci. Comput.* **20**, 907 (1998).
14. K. G. Powell, A tree-based adaptive scheme for the solution of the equations of gas dynamics and magneto-hydrodynamics, *Appl. Numer. Math.* **14**, 327 (1994).
15. W. J. Rider, An adaptive Riemann solver using a two-shock approximation, *Comput. Fluids* **28**, 741 (1999).
16. C.-W. Shu, Total-variation-diminishing time discretizations, *SIAM J. Sci. Stat. Comput.* **9**, 1073 (1988).
17. P. K. Smolarkiewicz, Comment on "a positive definite advection scheme obtained by nonlinear renormalization of the advective fluxes," *Mon. Weather Rev.* **117**, 2626 (1989).
18. P. K. Smolarkiewicz and L. G. Margolin, MPDATA: A finite-difference solver for geophysical flows. *J. Comput. Phys.* **140**, 459 (1998).
19. P. K. Sweby, High resolution schemes using flux limiters for hyperbolic conservation laws, *SIAM J. Numer. Anal.* **21**, 995 (1984).
20. E. F. Toro, *Riemann Solvers and Numerical Methods for Fluid Dynamics: A Practical Introduction*. (Springer-Verlag, Berlin/New York, 1997).
21. B. van Leer, Towards the ultimate conservative difference scheme. II. Monotonicity and conservation combined in a second-order scheme, *J. Comput. Phys.* **14**, 361 (1974).
22. B. van Leer, Towards the ultimate conservative difference scheme. IV. A new approach to numerical convection, *J. Comput. Phys.* **23**, 276 (1977).
23. B. van Leer, Towards the ultimate conservative difference scheme. V. A second-order sequel to Godunov's method, *J. Comput. Phys.* **32**, 101 (1979).
24. P. Woodward and P. Colella,The numerical simulation of two-dimensional fluid flow with strong shocks. *J. Comput. Phys.* **54**, 115 (1984).
25. S. T. Zalesak, Fully multidimensional flux-corrected transport algorithms for fluids, *J. Comput. Phys.* **31**, 335 (1979).